CHAPTER 12

NONLINEAR COUPLING IN WAVES PROPAGATING OVER A BAR

Y. Eldeberky[1] and J.A. Battjes[2]

Abstract

The degree of nonlinear coupling in a random wavefield propagating over and beyond a bar is examined using a physical wave flume as well as numerical simulations based on time-domain extended Boussinesq equations and their frequency-domain counter-part. The nonlinear phase speed is computed from the evolution of the nonlinear part of the phase function inherent in the frequency-domain model. Over the bar, the phase speeds of the higher harmonics are larger than the linear estimates due to the nonlinear couplings, resulting in virtually dispersionless propagation, while beyond the bar crest, nonlinear effects on the phase speed vanish rapidly, implying full release of bound harmonics. Quantitative measures of nonlinearity such as the skewness and asymmetry have also been determined. They have near-zero values in the deep-water region on either side of the bar and a pronounced peak over the bar. On the downwave side, the random wave field is found to be spatially homogeneous. This implies that it can be fully described by the energy density spectrum without additional phase information related to the bar location.

1. Introduction

The research described in this contribution deals with the propagation of nonbreaking waves over a shallow bar. It is aimed at investigating the degree of nonlinear coupling as waves evolve over and beyond a bar region. It is a continuation of previous related work by the authors on this subject (Eldeberky and Battjes, 1994).

---

[1]Research Assistant, [2]Professor at Delft University of Technology, Department of Civil Engineering, Section Hydraulics, Stevinweg 1, P.O. Box 5048, 2628 CN Delft, Netherlands

The conventional viewpoint is that on the seaside, the harmonics, bound to the primary, are amplified because of the increasing nonlinearity in the shoaling region, and that they are released on the shoreside, at least partially, because of the decreasing nonlinearity in the deepening region. Strictly speaking, however, even in the shoaling region free components are generated as a result of the nonhomogeneity, whereas conversely some degree of phase coupling may remain in the deepening region.

The phenomena mentioned above can with reasonable accuracy be modelled with Boussinesq-type equations, but these are unwieldy in applications involving wave propagation over large distances, for which phase-averaged, energy-based models with linear propagation are better suited. It is then convenient to switch to such a model at some distance downwave from the bar. Two questions then arise:
(1) How far downwave do the nonlinearities extend with non-negligible intensities? The answer to this question determines whether and from where the switch to a linear propagation model is justified.
(2) Are the fixed phase relations between harmonics, which are induced in the bar region, noticeable on the downwave side of the bar? If so, the wavefield on the downwave side of the bar would be spatially nonhomogeneous, with a "memory" of what happened over the bar (although the local nonlinear exchanges may already have vanished). This phenomenon is to be expected for wavefields with a discrete spectrum of only a few harmonics, but we expect that these effects cancel out in case of a continuous spectrum. If this is indeed the case, the wavefield shoreward of the bar would again be statistically homogenous. Knowledge of the energy spectrum on the downwave side (including the harmonics generated over the bar) would then be sufficient to characterize the wave field in a statistical sense, without additional phase information from "upwave" regions expressing the distance downwave from the bar.

The purpose of this paper is to investigate the questions raised above in a quantitative manner. This is done by determining the values and spatial distributions of the nonlinear contributions to the phase speed and of the skewness and asymmetry parameters, which are quantitative measures of nonlinearity.

The paper is arranged as follows. In section 2, the experimental arrangement is described. In section 3, the model equations used in the numerical simulations are presented. The analyses using the measures of nonlinearity followed by some results are given in section 4. Finally, section 5 presents the summary and conclusions.

2. Experimental Approach

Experiments with random waves reported by Beji and Battjes (1993) have yielded time series of surface elevation at a number of stations over a bar (still-water

depth 0.10 m) and on either side of it (still-water depth 0.40 m) (Fig. 1). A mechanical wave maker was used to generate wave signals according to a prescribed spectrum. The target spectrum was narrow-banded with peak frequency of 0.40 Hz and variance of 0.35 cm². At the downwave side, a beach with 1:20 slope was used as an absorbing boundary. Surface elevations were measured at stations 1 to 8 (the other stations refer to the numerical simulations). Station 1 is at the beginning of the upslope side of the bar, station 2 is 5.0 meters from station 1, and stations 3 to 8 are positioned every 1.0 meter.

These measurements have been analyzed to address the questions raised above. The analyses are mainly in the frequency-domain. Power spectra for these observations indicated significant transfer of energy from the spectral peak to higher frequencies (Beji and Battjes, 1993). Bispectral analysis showed the intensity and the spectral distribution of nonlinear couplings (Eldeberky and Battjes, 1994). Here we focus on the total measures of nonlinearity such as the skewness and asymmetry in order to investigate the spatial variation in the intensity of nonlinear couplings.

Due to the fact that the spatial coverage of the experimental data (up to station 8) is not enough to examine nonlinearity beyond the bar, a numerical "wave flume" has been employed to obtain results farther downwave. This is done using the time- and frequency-domain extended Boussinesq equations. The model equations are presented in the next section.
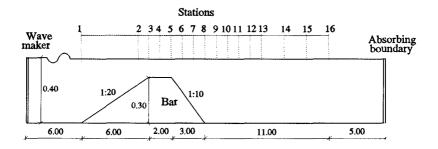

Fig. 1. Definition sketch of wave flume and location of wave gauges. All distances are expressed in meters

3. Numerical Approach

3.1 Time-domain model

Numerical simulations were performed using a 1-D extended Boussinesq model (Beji and Battjes, 1994) with improved dispersion characteristics, as in Madsen and Sørensen (1992), describing relatively long, small amplitude waves

propagating in water of slowly varying depth:

$$\frac{\partial u}{\partial t} + u\frac{\partial u}{\partial x} + g\frac{\partial \xi}{\partial x} = \frac{2}{5}h^2\frac{\partial^3 u}{\partial x^2 \partial t} + h\frac{\partial h}{\partial x}\frac{\partial^2 u}{\partial x \partial t} + \frac{1}{15}gh^2\frac{\partial^3 \xi}{\partial x^3} \quad , \quad (1)$$

$$\frac{\partial \xi}{\partial t} + \frac{\partial}{\partial x}[(h+\xi)u] = 0 \qquad (2)$$

Here, ξ is the surface displacement, u the depth-averaged horizontal velocity, h the still water depth, and g the gravitational acceleration. This set of equations has been integrated numerically using a difference scheme as described by Beji and Battjes (1994).

In the computation, the initial condition used is the unperturbed state. At the upwave boundary (station 1), the surface elevation is set equal to the experimental values; velocity values are derived from these using the long-wave approximation. At the outgoing boundary, an absorbing boundary condition has been used to ensure that the disturbances leave the computational domain without reflection.

3.2 Frequency-domain model

Numerical simulations were also performed using the frequency-domain counter part of the extended Boussinesq equations mentioned above. For one-dimensional propagation considered so far, the time (t) variation of the surface elevation (ζ) at each location (x) is expanded in a Fourier series as in

$$\xi(t;x) = \sum_{p=-\infty}^{\infty} A_p(x) \exp\{i(\omega_p t - \psi_p(x))\} \qquad (3)$$

with A_p denoting a complex amplitude, p indicating the rank of the harmonic, $\omega_p = p\omega_1$, and $d\psi_p/dx = k_p$, the wave number corresponding to ω_p according to the dispersion equation for the linearised Boussinesq equations. By substituting (3) into the time-domain Boussinesq equations, and by neglecting certain higher-order terms on the assumption of a sufficiently gradual evolution of the wave field, Madsen and Sørensen (1993) develop a set of coupled evolution equations for the set of complex amplitudes A_p which in abbreviated form can be written as

$$\frac{dA_p}{dx} = L_p\frac{dh}{dx}A_p + \sum_{m=1}^{p-1} Q_{m,p}^+ A_m A_{p-m} + \sum_{m=1}^{\infty} Q_{m,p}^- A_m^* A_{p+m} \qquad (4)$$

The first term on the right represents linear shoaling, proportional to the bottom slope dh/dx, the second term the triad sum interactions and the third the triad difference interactions. Complete expressions for the coefficients L, Q^+ and Q^- can be found in Madsen and Sørensen (1993). For the numerical integration of the evolution equation (4) and the applications to random waves with a given energy spectrum refer to Battjes et al. (1993).

4. Analysis

4.1 Phase speed

The evolution equation of the frequency-domain model is formulated in terms of complex Fourier amplitudes that contain the nonlinear part of the phase function. This equation (4) is used to obtain an evolution equation for the nonlinear part of the phase function in order to derive and evaluate a nonlinear correction to the linear phase speed. To this end, we express the complex amplitude $A_p(x)$ in its magnitude $a_p(x)$ and its phase $\alpha_p(x)$:

$$A_p(x) = a_p(x) e^{i\alpha_p(x)} \qquad (5)$$

After straightforward algebra, we obtain the following phase evolution equation for each harmonic after omitting the x-dependency for abbreviation,

$$a_p \frac{d\alpha_p}{dx} = \Im\left[\frac{dA_p}{dx}\right] \cos\alpha_p - \Re\left[\frac{dA_p}{dx}\right] \sin\alpha_p \qquad (6)$$

The values of a_p, α_p, and dA_p/dx at each location can be obtained from the numerical integration of equation (4). The phase speed of each harmonic, linear $(c_p)_l$ and nonlinear $(c_p)_{nl}$, can be obtain as follows

$$(c_p)_l = \frac{\omega_p}{(k_p)_l} = \frac{\omega_p}{d\psi_p/dx} \qquad (7)$$

$$(c_p)_{nl} = \frac{\omega_p}{(k_p)_{nl}} = \frac{\omega_p}{d\psi_p/dx + d\alpha_p/dx} \qquad , \qquad (8)$$

where $(k_p)_l$ and $(k_p)_{nl}$ are the linear and nonlinear phase change per unit length.

To examine the intensity of nonlinear coupling, the nonlinear phase speeds are compared to the linear predictions obtained from the extended Boussinesq equations.

For random incident waves, assumed to have independent, random phases at station 1, Fig. 2 shows the spectral densities, the linear and the nonlinear phase speeds at different locations over the bar. Over the upslope of the bar (station 2), the nonlinear phase speeds of the higher harmonics are larger than the linear estimates due to the nonlinear couplings to the primary. Over the bar crest (station 4), the nonlinear phase speeds are nearly constant and equal to $\sqrt{gh}$ (nondispersive shallow-waves). Beyond the bar (station 8), the nonlinear predictions of phase speed agree with the linear estimates, implying full release of bound harmonics. The results farther beyond the bar (not shown here) did not show any deviation in the nonlinear phase speeds from the linear predictions, implying the absence of nonlinear couplings. Likewise, the energy spectrum of

the waves did not evolve in the region beyond the bar. This in turn means that nonlinear models are not needed to characterize the wavefield beyond the bar.
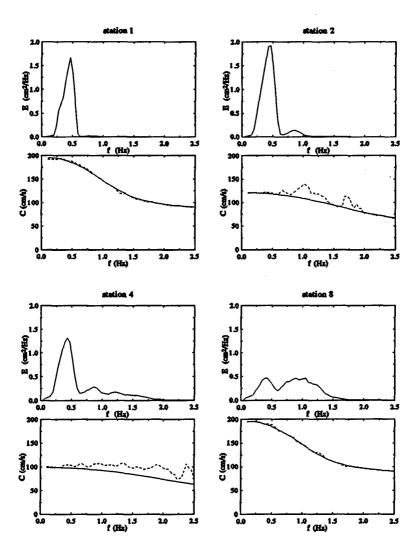

Fig. 2. Computed energy density spectra (upper panels), linear (solid line) and total (dashed line) phase speeds (lower panels) at stations 1, 2, 4, and 8

4.2 Skewness and Asymmetry

To measure the nonlinearities associated with the nonlinear couplings, higher-order moments are needed such as the skewness and asymmetry. These are measures of asymmetry of the wave profile around the horizontal (crest to trough asymmetry) and the vertical (front to back asymmetry) plane respectively. Skewness and asymmetry values have been computed according to the definitions given by Hasselmann *et al.* (1963) and Elgar and Guza (1985) respectively.

The original wave flume and its numerical simulation
The skewness and asymmetry have been computed for both the measured and time-domain computed surface elevations at various locations over the bar. Their variations are given in Fig. 3. The comparison shows the ability of the numerical model to reproduce the nonlinear evolution of waves propagating in varying water depth with sufficient accuracy for the present purpose.

The variations indicate a significant increase on the upslope to a maximum over the bar. To the lee of the bar crest, the skewness and asymmetry decrease rapidly to near-zero values, comparable to those on the exposed side of the bar. (For skewness values less than 0.2, Ochi and Wang (1984) found virtually no deviation from the Gaussian probability density of the sea surface elevation.) This in turn means absence of significant nonlinear interactions at the downwave side of the bar. We expect that for random waves with a continuous spectrum, this will imply spatial homogeneity. This is checked below by using computed signals in the region beyond that of the measurements.
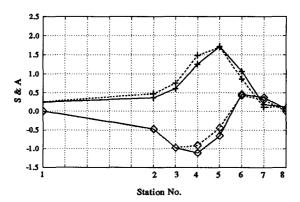

Fig. 3. Skewness (+) and asymmetry (◊): comparison between results from the physical wave flume (solid lines) and the numerical wave flume (dashed lines)

Numerical simulation for extended region
Time-domain numerical computations have been performed extending to distances
farther downwave in order to examine the homogeneity of the wavefield in that
region. The computational domain now extends to station 16; the distances
between stations 9 to 13 are 1.0 m and those between stations 14 to 16 are 2.0 m.

Computations are done for two different upwave boundary conditions,
corresponding to sinusoidal and irregular waves. The former is to demonstrate
the spatial nonhomogeneity associated with the interference between a primary
wave and its harmonics. The latter is to investigate the matter for the case of a
continuous spectrum, where the innumerable interferences are expected to cancel,
resulting in a homogeneous wavefield.
To demonstrate the contrast between the two cases, the nonlinearity parameter
(*a/h*) is kept constant by imposing the same surface elevation variance at the
upwave boundary. The computations are performed for the same record duration
as in the physical experiment, and the computed signals at stations 1 to 16 have
been analyzed in the frequency-domain in the same manner as the experimental
records.

Sinusoidal waves
Fig. 4 shows the spatial variations of the amplitudes of the primary wave and its
harmonics. Over the bar, a significant energy transfer takes place into the second,
third and fourth harmonics. Beyond the bar, the amplitudes do not vary because
of absence of nonlinear interactions.

The corresponding variations in the skewness and asymmetry are shown in Fig.
5. They indicate a significant increase on the upslope to a maximum over the bar
as a result of harmonic generation. On the downslope side of the bar, the
skewness and asymmetry decrease rapidly to values between ±0.5. Beyond the
bar, although the amplitudes of the harmonics are nearly constant, the skewness
and asymmetry vary significantly as a result of the varying phase lags between
the freely propagating component-waves, resulting in a spatially nonhomogenous
wavefield.

Irregular waves
Fig. 6 shows the variations of skewness and asymmetry over the upslope, the bar
crest, the downslope and farther downwave; the latter is of particular interest
here. It shows that over the horizontal region, and in contrast to the case of
sinusoidal waves, the skewness and asymmetry remain at near-zero values (less
than 0.2), comparable to those on the exposed side of the bar, without any
significant spatial variations. This implies that there is no memory of the bar
location, in contrast to the discrete case. The practical implication of this is that
the waves downwave from the bar can again be assumed to have independent,
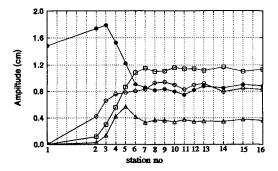random phases.

*Fig. 4. Spatial variations of the amplitudes of the primary wave and its harmonics
primary wave (●), second harmonic (○), third harmonic (□), and fourth harmonic (△)*
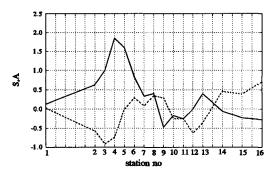

*Fig. 5. The spatial variations of skewness (solid line) and asymmetry (dashed line) for
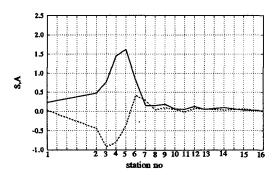sinusoidal incident waves (at station 1)*

*Fig. 6. The spatial variations of skewness (solid line) and asymmetry (dashed line) for
irregular waves*

5. Summary and Conclusions

The degree of nonlinear coupling as waves evolve over and beyond a bar is examined. The extended Boussinesq equations that had shown success in this kind of application are used in this investigation together with experimental data. The situation considered was such that significant harmonic generation took place on the upslope leading to the bar crest. The following indicators of nonlinearity were used: the nonlinear phase speed, the skewness and asymmetry. Inspection of their spatial variations has led to the following conclusions.

- The comparison between linear and nonlinear estimates of the phase speeds indicates that over the bar, the bound harmonics travel faster than their corresponding free waves that have linear phase speeds. Beyond the bar, they propagate with the linear phase speed implying that they are fully released.

- The skewness and asymmetry have near-zero values in the deep-water region on either side of the bar and a pronounced peak over the bar. On the downwave side, the wavefield is found to be spatially homogeneous for irregular waves without memory of the phase couplings which existed over the bar crest. This is in contrast to the case of a discrete, finite set of wave components.

Summarizing, the wavefield on the downwave side is virtually linear and statistically homogeneous. It can be fully described by the energy density spectrum with linear propagation, and without the need for additional phase information reflecting the site-dependent distance downwave from the bar.

Acknowledgements

References

Beji, S., and Battjes, J.A. (1993). Experimental investigation of wave propagation over a bar. *Coastal Eng.*, 19, 151-162.
Beji, S., and Battjes, J.A. (1994). Numerical simulation of nonlinear waves propagating over a bar. *Coastal Eng.*,23, 1-16.
Battjes, J.A., Eldeberky, Y., and Won, Y. (1993). Spectral Boussinesq modelling of breaking waves. *Proc. Int. Conf. WAVES '93*, New Orleans, ASCE, pp. 813-820, New York.
Eldeberky, Y., and Battjes, J.A. (1994). Phase lock in waves passing over a bar. *Proc. Int. Sym. WAVES-PHYSICAL AND NUMERICAL MODELLING*

'94, Vancouver, pp. 1086-1095.

Elgar, S. and Guza, R.T. (1985). Observations of bispectra of shoaling surface gravity waves. *J. Fluid Mech.*, Vol. 161, 425-448.

Hasselmann, K., Munk, W., and McDonald, G. (1963). Bispectra of ocean waves. In: *Time Series Analysis* (edited by M. Rosenblatt), 125-139, Wiley, New York.

Madsen, P.A., and Sørensen, O.R. (1992). A new form of the Boussinesq equations with improved linear dispersion characteristics. Part 2: a slowly-varying bathymetry. *Coastal Eng.*, 18, 183-205.

Madsen, P.A., and Sørensen, O.R. (1993). Bound waves and triad interactions in shallow water. *J. Ocean Eng.*, 20 (4), 359-388.

Ochi, M.K. and Wang, W.C. (1984). Non-Gaussian characteristics of coastal waves. *Proc. 19th Int. Conf. on Coastal Eng.*, Houston, Vol.1, pp.516-531